Three-dimensional numerical simulation of mortar and concrete model failure in meso level by Rigid Body Spring Model

Kohei NAGAI*, Yasuhiko SATO**, Tamon UEDA***

*M. of Eng., Doctoral Course, Div. of Structural and Geotechnical Eng., Hokkaido University, Sapporo, 060-8628
**Dr. of Eng., Associate Researcher, Div. of Structural and Geotechnical Eng., Hokkaido University, Sapporo, 060-8628
***Dr. of Eng., Associate Professor, Div. of Structural and Geotechnical Eng., Hokkaido University, Sapporo, 060-8628

Concrete is a heterogeneity material consisting of mortar and aggregate in meso level. Evaluation of fracture process in this level is useful to clarify the material characteristic of concrete. However, analytical approach in this level has not been carried out enough yet. In this study, three-dimensional analyses of compression and tension test of mortar and compression test of concrete model are carried out by Rigid Body Spring Model (RBSM). In the compression and tension analysis of mortar, fracture process and failure pattern can simulate well usual experimental results. And the effect of boundary condition in the compression test on the fracture pattern is simulated reasonably. In the analyses of the concrete model, effect of the existence of aggregate model can be predicted qualitatively. These results show the possibility of 3D RBSM analysis to predict the concrete behavior quantitatively in various cases in the future.

Key Words: 3D RBSM, meso-scopic analysis, concrete model, Voronoi geometry

1. Introduction

Estimation of durability of concrete structure in long time span that is affected by the various environmental and mechanical loading conditions becomes an important factor for the efficient and economical construction and maintenance of concrete structures. Study on concrete in meso level in which concrete is consisting of mortar and aggregate is useful for the precise evaluation of its material characteristics that are affected by those of components. And also the deterioration of the material characteristics of damaged concrete by an environmental action can be predicted by the analysis from this level in the future.

Many experimental researches were conducted on fracture mechanism in meso level in the past. In these researches, fracture propagation from the interface between mortar and aggregate to the mortar part is observed in compression test and the effect of the aggregate on nonlinearity of macro-scopic stress-strain curve of concrete and the failure of concrete are mentioned[1) 2) 3)]. In recent years, researches in meso level from the analytical point of view have started but not been conducted enough yet[4) 5)]. Especially the analysis of compression test has hardly been carried out due to its complicated failure behavior[6) 7)]. Furthermore, discrete three-dimensional analysis is necessary to present the three-dimensional fracture propagation between aggregates three-dimensionally arranged in concrete.

In this study, three-dimensional numerical simulations of fracture process of compression and tension test of mortar and compression test of concrete model where shape of the aggregate model is sphere are conducted by 3D Rigid Body Spring Model (RBSM). This analysis method is useful to simulate a discrete behavior like concrete fracture. In other than concrete field, Toi et al. has studied on damage mechanics model by 3D RBSM [8) 9)]. The authors had developed a two-dimensional RBSM analytical system and constitutive models for mortar and mortar-aggregate interface in meso level[10) 11)]. The constitutive model in 3D RBSM is developed in this study based on that in 2D.

In this paper, only the uniaxial compression and tension tests are carried out. Analyses under biaxial and triaxial loading condition of concrete will be conducted in the future to simulate the dependence of hydrostatic pressure of concrete.

2. Method of numerical analysis

The RBSM developed by Kawai[12)] is one of discrete numerical analysis method. Analytical model is divided into polyhedron elements whose phases are interconnected by springs. Each element has three transitional and three

rotational degrees of freedom at the center of gravity. One normal and two shear springs are placed at the center of gravity of each phase (Fig.1). Since cracks initiate and propagate along the boundary phase, the mesh arrangement may affect fracture direction. To avoid formation of cracks with a certain direction, a random geometry is introduced using a three-dimensional Voronoi diagram (Fig.2). The Voronoi diagram is the collection of Voronoi cells. Each cell represents mortar or aggregate element in the analysis.

In the nonlinear analysis, stiffness matrix is constructed by the principle of virtual work[12], and the Modified Newton-Raphson method is employed for the convergence algorithm. When the model does not converge at the given maximum iterative calculation number, analysis proceeds to next step.

3. Constitutive model

3.1 Mortar model

In this study, a constitutive model for mortar in meso level is developed because the constitutive model in macro scale cannot be applied to meso scale analysis.

Material characteristics of each component are presented by means of modeling springs. In normal springs, compressive and tensile stresses (σ) are developed. Shear springs develop shear stresses (τ). For the calculation of shear stress, a resultant value of strains generated in two shear springs is adopted as a shear strain in the constitutive model presented in this section.

Elastic modulus of springs are presented assuming plane strain condition,

$$k_n = \frac{(1-\nu_{elem})E_{elem}}{(1-2\nu_{elem})(1+\nu_{elem})}$$
$$k_s = \frac{E_{elem}}{2(1+\nu_{elem})} \quad (1)$$

where k_n and k_s are the elastic modulus of normal and shear spring, E_{elem} and ν_{elem} are the corrected elastic modulus and Poisson's ratio of component for meso level, respectively.

In the analysis, due to the random geometry of the elements, values of the material property, which are the material property in meso level, given to the element are different from those of the analyzed object as the macro-scopic material property. In this study, the material properties for the element were determined in such a way to give the correct macro-scopic properties. For this purpose, the elastic analysis of mortar in compression was carried out. In discrete analysis such as RBSM, shape of elements

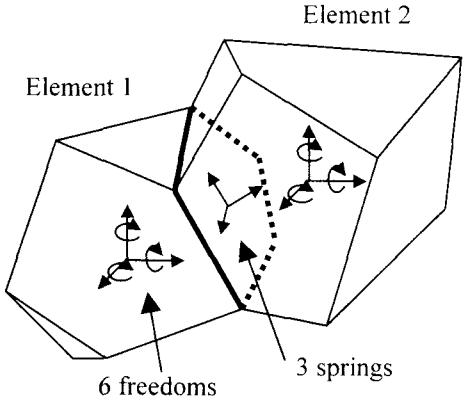

Fig. 1 Mechanical model

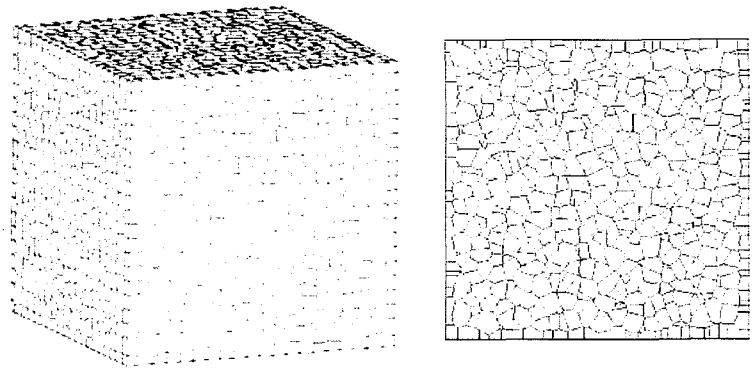

a) 3D view b) Cross section

Fig. 2 3D Voronoi geometry

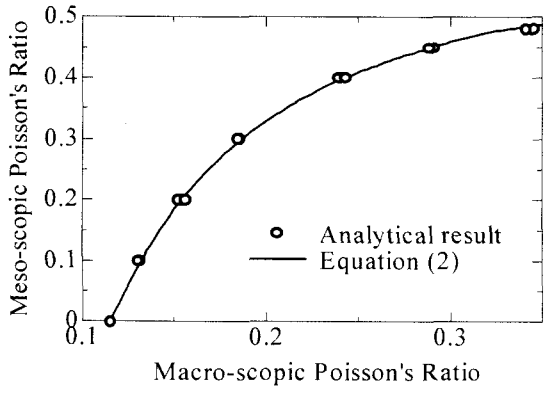

a) Poisson's ratio

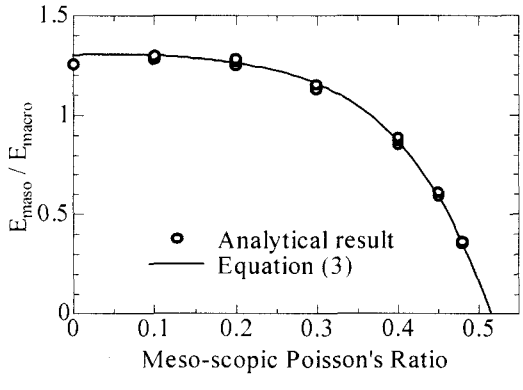

b) Elastic modulus

Fig. 3 Effect of meso-scopic material properties on macro-scopic material properties

and element fineness affect the result of analysis[13]. To reduce these effects, small size of element is adopted and element fineness in all analyses are almost same level that is about 2.5~3.0mm^3/1element in this study. In the elastic analyses, the relationship between the macro-scopic and meso-scopic Poisson's ratio and the effect of the meso-scopic Poisson's ratio on the macro-scopic elastic modulus were examined. From the results (Fig.3), Eq.(2) and Eq.(3) are adopted for determining the meso-scopic material properties.

$$\nu_{elem} = -237.0\nu^4 + 266.6\nu^3 - 116.1\nu^2 + 24.1\nu - 1.6 \quad (0.12 \leqq \nu \leqq 0.35) \quad \cdots\cdots (2)$$

$$E_{elem} = \left(-41.5\nu_{elem}^{\ 4} + 21.1\nu_{elem}^{\ 3} - 5.5\nu_{elem}^{\ 2} + 0.4\nu_{elem} + 1.3\right)E \quad \cdots\cdots (3)$$

where E and ν are macro-scopic elastic modulus and Poisson's ratio of component of analyzed object, respectively.

Only the maximum tensile stress has to be set as a material strength. Actually, mortar itself is not a homogeneous material, which is consisting of sand and paste, even when bleeding effect is ignored. However strength distribution in mortar has not been clarified yet. In this study, a normal distribution is assumed for the tensile strength on element boundary. The probability density function is as follows (Fig. 4),

$$f(f_{t\,elem}) = \frac{1}{\sqrt{2\pi}} \exp\left\{-\frac{\left\{3(f_{t\,elem}/f_{t\,average}-1)\right\}^2}{2}\right\}$$

when $f_{t\,elem} < 0$ then, (4)

$$f_{t\,elem} = 0$$

where $f_{t\,elem}$ is distributed tensile strength and $f_{t\,average}$ is average tensile strength of mortar in meso level. And also, the same distribution is given to the elastic modulus. Those distributions affect the macro-scopic elastic modulus, so that the elastic modulus for the element is multiplied by 1.05.

Springs set on the phase act elastic until generated stresses reach τ_{max} criterion as follows,

$$\varepsilon = \frac{\Delta n}{h_1 + h_2}$$
$$\gamma = \frac{\Delta s}{h_1 + h_2} \quad (5)$$
$$\sigma = k_n \varepsilon$$
$$\tau = k_s \gamma$$

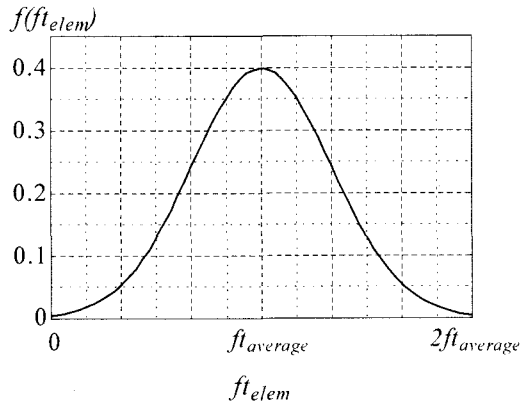

Fig. 4 Distribution of material properties

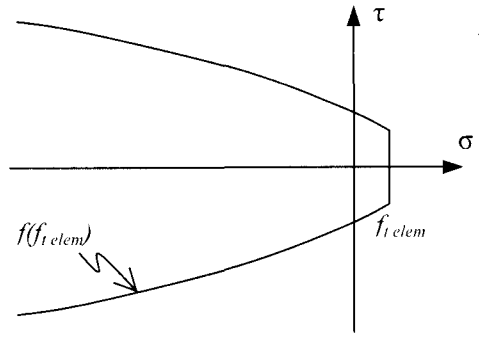

Fig. 5 τ_{max} criterion for mortar

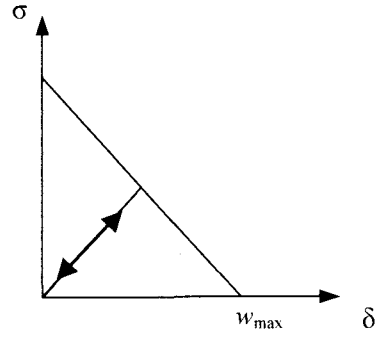

Fig.6 Tensile softening model for mortar

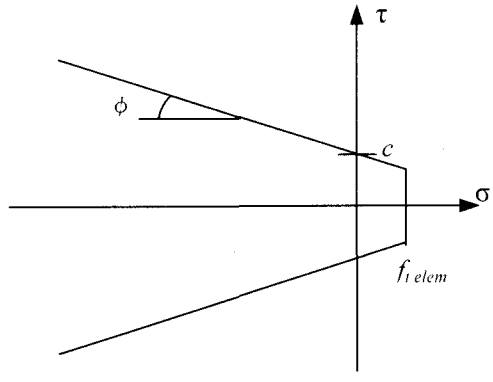

Fig. 7 τ_{max} criterion for interface

where ε and γ are the strain of normal and shear springs, respectively. Δn and Δs are the normal and shear relative displacement of elements those compose springs, respectively. h is the length of perpendicular line from the center of gravity of element to the boundary. And subscripts 1 and 2 represent elements 1 and 2 in Fig.1, respectively. τ_{max} criterion is given as shown in Eq.(6) and Fig.5.

$$\tau_{\max} = \pm\left\{0.08 f_{telem}{}^{2.7}\left(-\sigma + f_{telem}\right)^{0.7} + f_{telem}\right\} \quad (\sigma < f_{telem}) \qquad \cdots\cdots \quad (6)$$

When a generated spring stress goes beyond τ_{max}, the shear stress(τ) is reduced to τ_{max} which depends on the normal stress(σ) in the range that the normal stress is less than $f_{t\,elem}$. τ_{max} can increase with increasing normal compressive stress. Stresses can be transferred only through the contact area of each boundary which is calculated by the shear displacement of elements constituting the boundary. Fracture happens between the elements when the normal stress reaches $f_{t\ elem}$, and the normal stress becomes dependent on crack width that is the spring elongation. Shear stress is also affected by the crack width. Both normal and shear stresses are assumed to decrease linearly with the crack width. Stresses after cracking are represented as follows,

$$\sigma = \frac{w_{\max} - w}{w_{\max}} f_{t\,elem} \qquad (w < w_{\max})$$

$$\sigma = 0 \qquad (w \geqq w_{\max})$$

$$\tau = \frac{w_{\max} - w}{w_{\max}} \tau_c \qquad (w < w_{\max}) \qquad (7)$$

$$\tau = 0 \qquad (w \geqq w_{\max})$$

where,

$$\tau_c = k_s \gamma \qquad (k_s \gamma \leqq f_{t\,elem})$$

$$\tau_c = f_{t\,elem} \qquad (k_s \gamma > f_{t\,elem})$$

where w is crack width and w_{max} is the maximum crack width which can carry stress. In this study, w_{max} is set 0.005mm. And the linear unloading and reloading path that goes through the origin is introduced to normal spring in tension zone (Fig.6).

In this study, normal springs in compression only behave elastically and never break nor have softening behavior.

3.2 Aggregate model

In this study, effect of existence of aggregate in concrete on fracture process is examined. For this purpose, element of aggregate behaves only elastic in this study. The same equations as (1), (2), (3) and (5) are adopted to present the material property of aggregate.

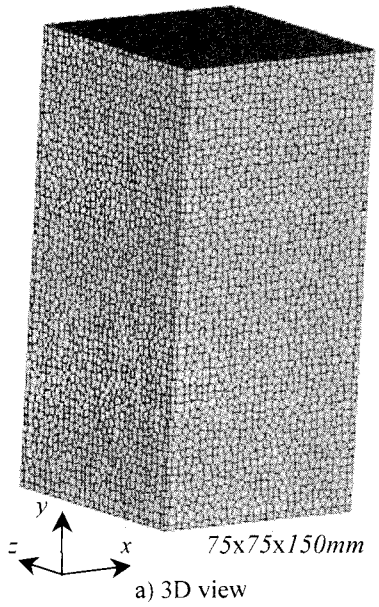

a) 3D view

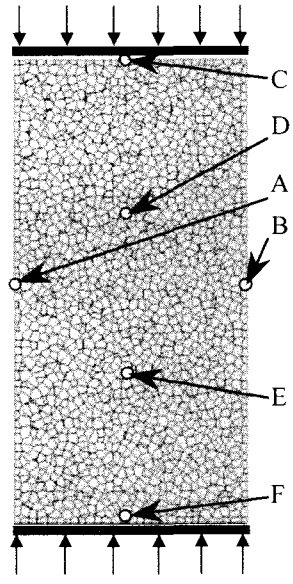

b) Cross-section at z=37.5mm

Fig. 8 Analytical model

Table 1 Input material properties of mortar

$f_{t\,average}$	4.2 MPa
Elastic modulus (E)	24,000 MPa
Poisson's Ratio (ν)	0.18

3.3 Interface model

The same stress-strain relationships as Eq.(5) and strength and stiffness distribution as Eq.(4) are adopted for the material properties of the interface between mortar and aggregate. The spring stiffnesses k_n and k_s of the interface are given by a weighted average of the material properties in two elements according to their perpendiculars. That is,

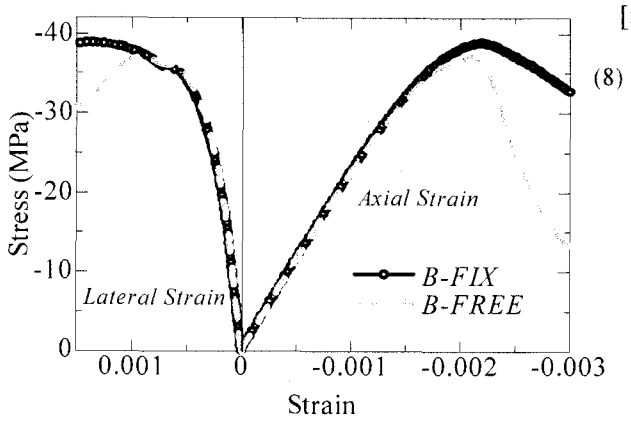

Fig. 9 Stress-strain curves in compression

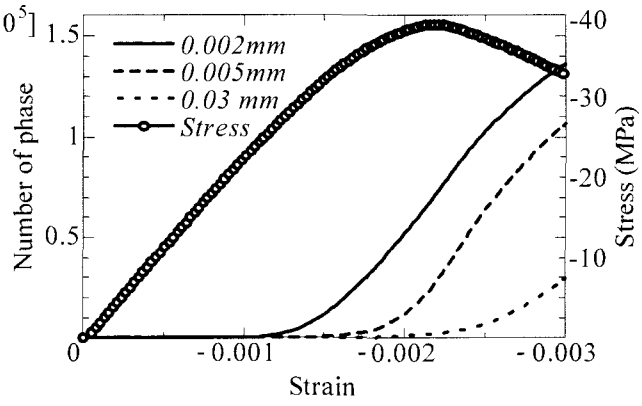

Fig. 10 Number of phase reaching crack width

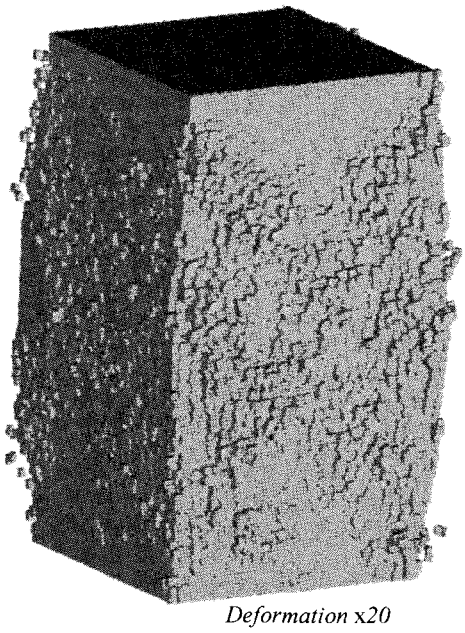

Deformation x*20*

a) Model B-FIX

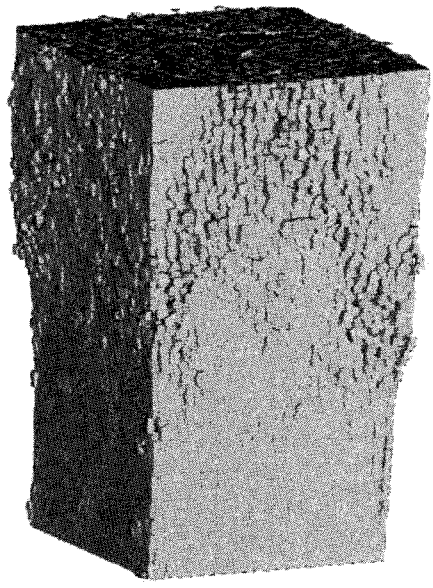

Deformation x*10*

b) Model B-FREE

Fig. 11 Deformations after peak stress in compression

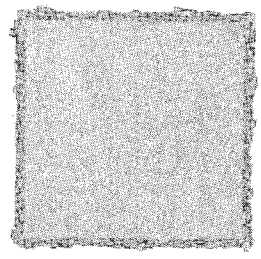

a) Model B-FIX

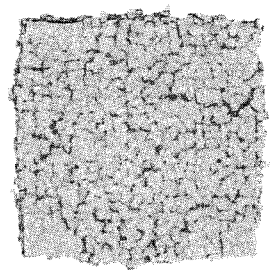

b) Model B-FREE

Deformation x*10*

Fig. 12 Views from the top after peak stress

$$k_n = \frac{k_{n1}h_1 + k_{n2}h_2}{h_1 + h_2}$$

$$k_s = \frac{k_{s1}h_1 + k_{s2}h_2}{h_1 + h_2}$$

where subscripts 1 and 2 represent elements 1 and 2 in Fig.1, respectively. For the interface between mortar and aggregate, the τ_{max} criterion as shown in Eq.(9) and Fig.7 is adopted.

$$\tau_{\max} = \pm(-\sigma \tan\phi + c) \qquad (\sigma < f_{telem}) \qquad (9)$$

where ϕ and c are constant values.

This criterion is based on the failure criterion suggested by Kosaka et al.[3] which is derived from experimental results. After stresses reach the failure criterion, the shear stress(τ) is reduced to τ_{max} which depends on the normal stress(σ) in the range where the normal stress is in compression zone. In the tension zone, both normal and shear stresses cannot transfer the stress after the stresses reach the criterion.

4. Analyses of mortar models

Numerical analyses of the mortar specimen in compression and tension are carried out. In compression analyses, 2 types of model are analyzed: (i) boundary of the top and bottom are fixed in lateral direction (B-FIX); and (ii) boundary not fixed in lateral direction (B-FREE). Fig.8 shows 3D view of numerical model and *x-y* cross-section at *z*=37.5mm. Size of the specimen is 75x75x150mm and number of mortar element is 48,778. Average element size is about 2.59mm^3. Material properties of mortar are set as shown in Table1 where only the tensile strength is set as the

strength of mortar. Number of the phase in which springs are set is 359,149 in the model.

4.1 Compression analyses

Fig.9 shows the predicted stress-strain relationships in the mortar compression test of model B-FIX and B-FREE. Lateral strains are calculated by the relative deformation between the elements at A and B in Fig.8. Strengths of the models are 38.87MPa and 37.08MPa in model B-FIX and B-FREE respectively. The strength of model B-FIX in compression is 8.7 times bigger than that of in tension (see Section 4.2) and this strength relationship is not far from the experimental results[11]. Predicted curves show nonlinearity in axial direction before 50% of maximum stress. Ratio of the lateral strain to the axial strain starts increasing rapidly around 70% of the maximum stress. These behaviors are observed in the experiments of mortar compression test as well[14) 15)]. Curves in Fig.10 show the number of phases whose crack widths reach 0.002mm, 0.005mm and 0.03mm in the simulation of model B-FIX. Horizontal axis shows the macro-scopic strain of the model. And also macro-scopic stress is presented in the graph. Number of the phases, whose crack widths become more than 0.005mm and cannot transfer the stresses any more, increases suddenly from around 85% of the maximum stress. This fact that sudden increase in crack causes the failure of model is the same as in usual experimental results. Fig.11 shows the model deformations after peak stress (at axial strain of -2,900μ). Deformations are enlarged 20 and 10 times, respectively. In model B-FIX, failure occurs in other than the vicinity of loading boundary and the damage around the loading boundary is less. On the contrary, cracks reach the loading boundary in model B-FREE. Views of models' deformation after the peak stress from the top in Fig.12 show the difference in fracture pattern more clearly. This difference is considered as a general effect of the loading boundary condition[16]. However, propagation of some main cracks that is observed in the usual experiment cannot be simulated in this study.

4.2 Tension analysis

Predicted stress-strain relationship in the tension analysis is shown in Fig.13. Macro-scopic tensile strength is 4.47MPa, which is similar to the average tensile strength set along the boundaries (see Section 3 and Table 1). The shape of stress-strain curve shows the nonlinearity before the peak stress as much as in compression. This behavior is observed in 2D analysis as well[11]. Further research is necessary. Fig.14 shows the deformation of the model at failure. The deformation is enlarged 50 times. Propagation of single crack that can be seen in usual experiments can be simulated. Fig.15 shows the average strains of every 50mm section in the axial direction. To calculate the strains of *Upper 50mm*, *Middle 50mm* and *Lower 50mm* in Fig.15, relative deformations between the elements at C and D, D and E, and E and F in Fig.8 are used respectively. The vertical axis shows the macro-scopic stress. Until the peak, similar curves are predicted. It means that the model extends uniformly. In the post peak range, only the strain in *Middle 50mm* where the single crack propagates (see Fig.14) increases and the strains in other sections reduce. This localization behavior in failure processes in tension is also observed in usual experimental result.

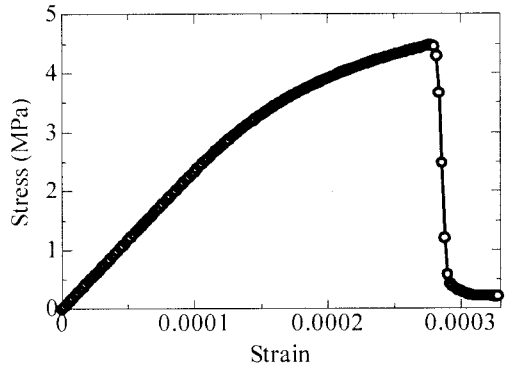

Fig. 13 Stress-strain curve in tension

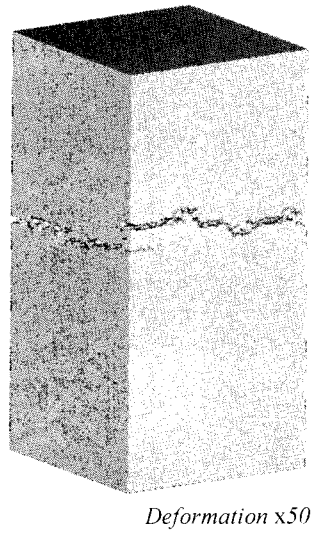

Fig. 14 Deformation at failure in tension

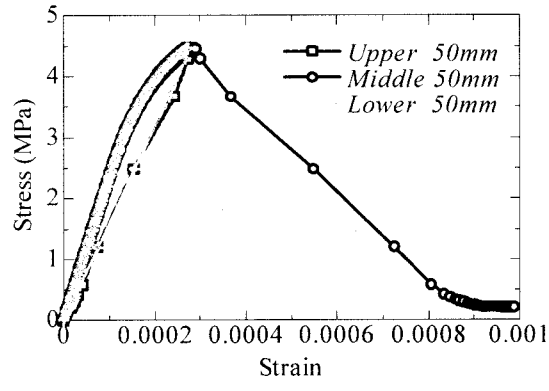

Fig.15 Strains in every 50mm in axial direction

5. Analyses of concrete models

To examine the effect of existence of aggregate in mortar and the behavior of the interface between mortar and aggregate, numerical analyses of compression tests of concrete model consisting of mortar and sphere aggregates are carried out. Two types of model are simulated: (i) the specimen with single sphere aggregate set at the center; (ii) the specimen with aggregates those size distribution is decided based on the JSCE Standard Specification for Concrete Structures. Sizes of the specimens are 75x75x150mm. Material property of the mortar is same as in the mortar analyses (see Table 1). And the material properties of the aggregate and interface between the mortar and aggregate are presented in Table 2. To decide

Table 2 Input material properties

Aggregate	
Elastic modulus (E)	50,000 MPa
Poisson's Ratio (ν)	0.25
Interface	
$f_{t\,average}$	1.6 MPa
c	2.7 MPa
ϕ	35°

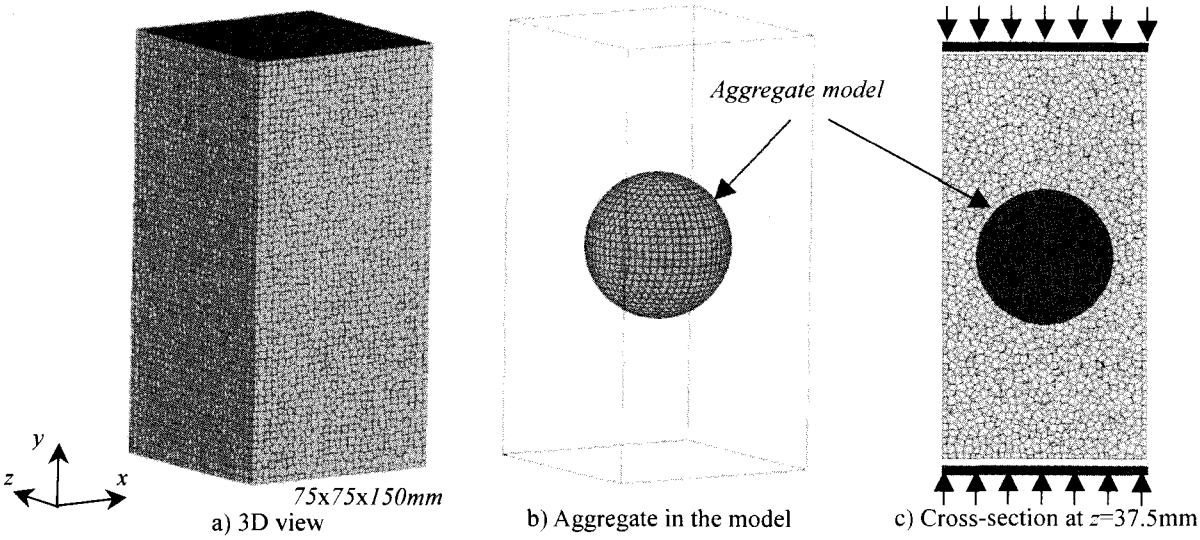

Fig. 16 Single aggregate concrete model

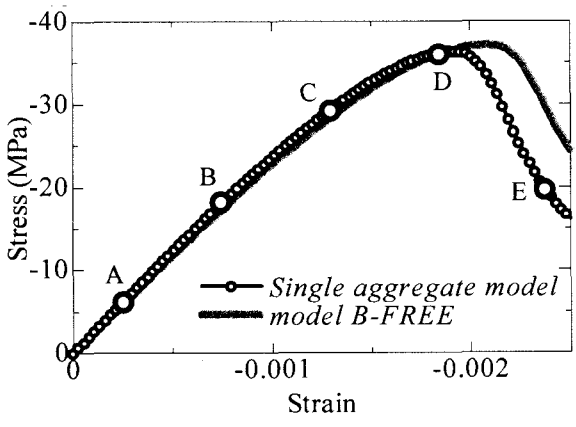

Fig. 17 Stress-strain curves

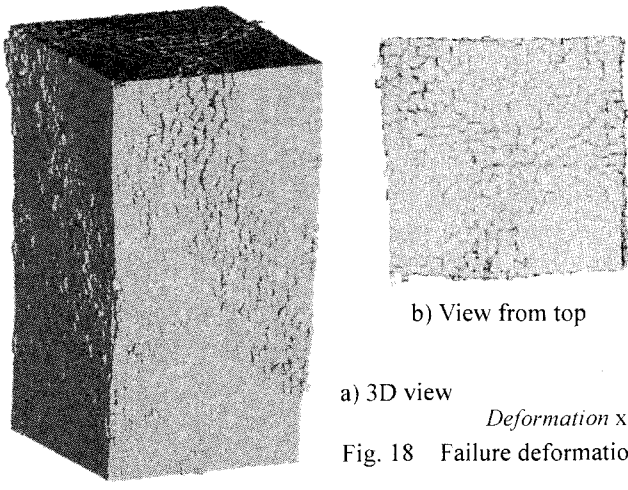

Fig. 18 Failure deformation

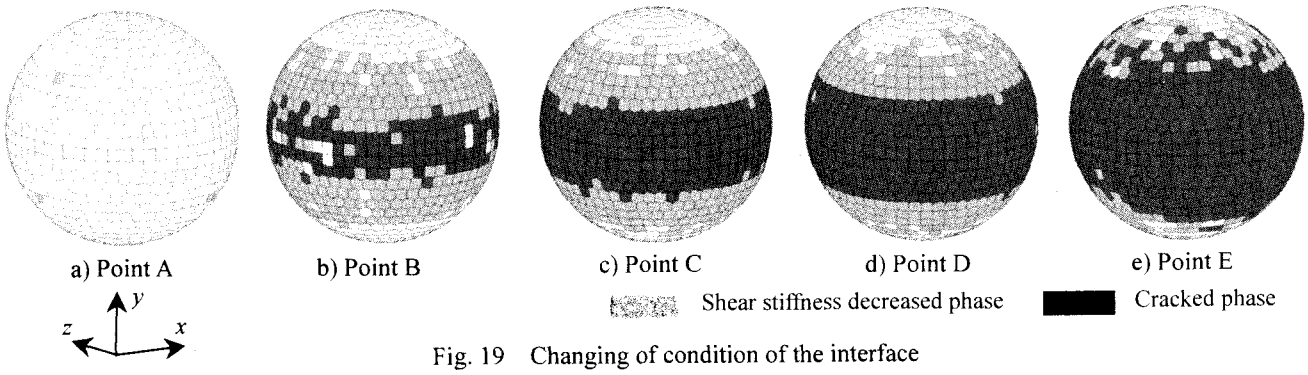

Fig. 19 Changing of condition of the interface

the material properties of the interface, researches conducted by Kosaka et al.[3], Michael A. Taylor et al.[17] and Thomas T. C. Hsu et al.[18] are referred and the general values are selected. Average size of the element is same as the mortar specimen, which is 2.59mm^3.

5.1 Single aggregate concrete model

Numerical model of the single sphere aggregate concrete model is shown in Fig.16 where 3D view of the model, 3D aggregate view in the model and *x-y* cross-section at *z*=37.5mm are presented. Diameter of the aggregate is 50mm. Only the shape of the phase on the aggregate surface is controlled to form the sphere aggregate (Fig.16 b)). In the compression analysis, the loading boundary is not fixed in lateral direction. Total number of the element is 48,790 including 3,895 aggregate elements.

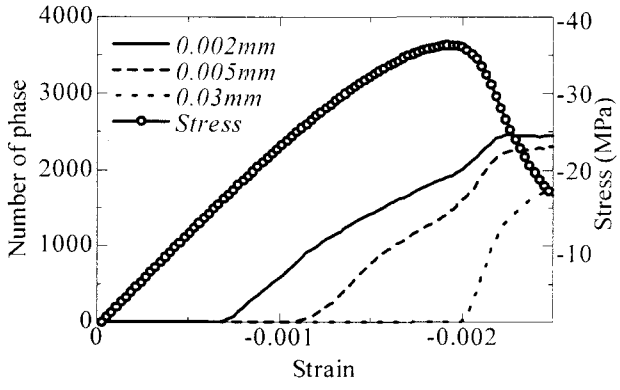

a) Interface

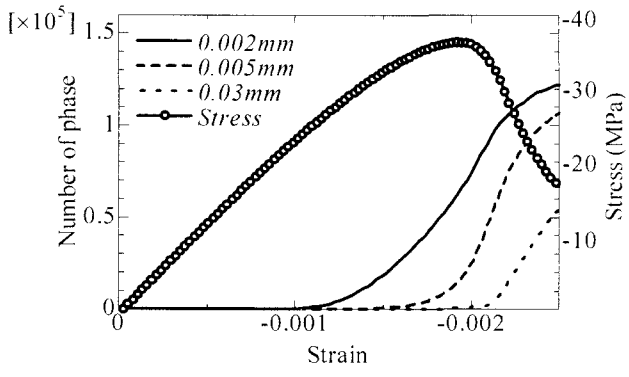

b) Mortar

Fig. 20 Number of phase reaching crack width

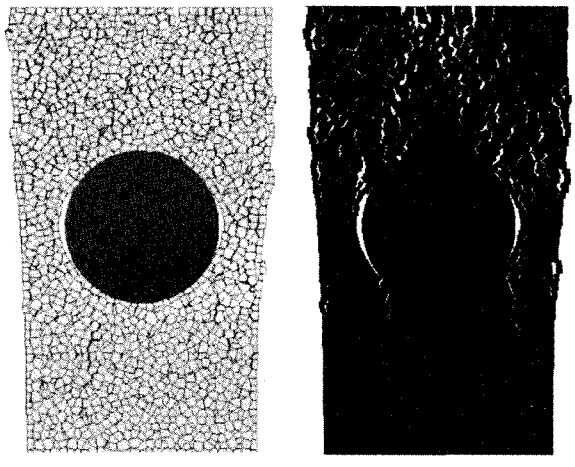

a) Presented by element b) Presented in black

Deformation x*10*

Fig. 21 Cross-section at *z*=37.5mm at failure

Fig.17 shows the predicted stress-strain curve. Simulated results of model B-FREE is presented as well. Strength of the concrete model is 36.28MPa. It decreases slightly compared with the mortar model B-FREE. Kosaka et al. did the experiment on single aggregate concrete model by the two-dimensional type experiment where cylindrical shape aggregate model is set at the center of the mortar part[3]. Though the shape of the aggregate in analysis is different, the fact that slight decrease of strength of the specimen with the single high strength aggregate is same as the experimental result. Fig.18 shows the failure deformation at point E in Fig.17. Deformation is enlarged 10 times. Same as the simulated result of model B-FREE (see Fig.11), cracks reach loading boundary. Fig.19 shows the changing of the interface condition at points A-E in Fig.17. Gray and black phases present the phases that reach the τ_{max} criterion in compression zone and tension zone, respectively. It means that the decrease of shear stiffness occurs on the gray phase and the crack happens on the black phase (See Section 3.3). The phases that reach the τ_{max} criterion in compression zone have already produced a band area on the side of aggregate in low stress level (Fig.19 b)). And the crack band area, which is presented by black phases, develops from point B to failure (Fig.19 b)-e)). In the two-dimensional type experiment of concrete model with high strength single aggregate conducted by Kosaka et al.[3], interface crack occurs on the side of aggregate and propagate from 54% of maximum stress of the model. Similar fracture propagation is simulated in the three-dimensional analysis. Fig.20 a) and b) show the increasing of numbers of phases of interface and mortar whose crack widths reach 0.002mm, 0.005mm and 0.03mm. Horizontal axis shows the macro-scopic strain of the model. And also macro-scopic stress is presented in the graphs. From the graphs, it is observed that the interface cracks occur and propagate from lower stress level than the mortar cracks. Fig.21 shows the *x-y* cross-section at *z*=37.5mm at failure (Point E in Fig.17). Deformation is enlarged 10 times. Interface crack on the side of the aggregate and the triangular non-cracking area of the mortar, which is a cone shape zone in 3D, above the aggregate are seen. This cone shape undamaged zone is observed in the experiment as well[19].

5.2 Concrete model

Analysis of the compression test of concrete model where sphere aggregates are introduced is conducted.

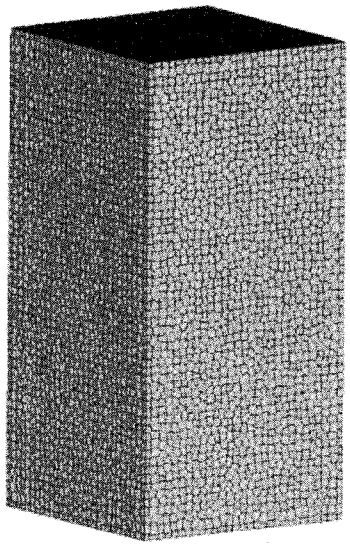

a) 3D view

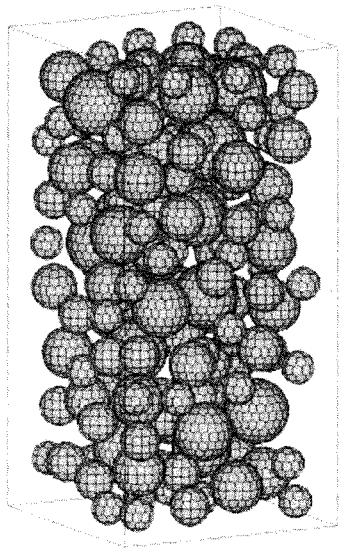

b) Aggregates in the model

Fig. 22 Concrete model

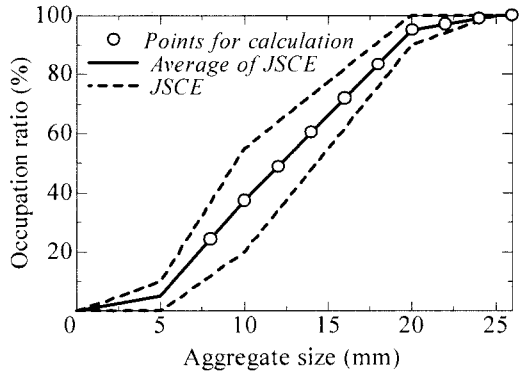

Fig. 23 Grain-size distribution

Table 3 Introduced aggregate

Size (mm)	Number
10	72
12	36
14	23
16	16
18	11
20	8
22	1
Total	167

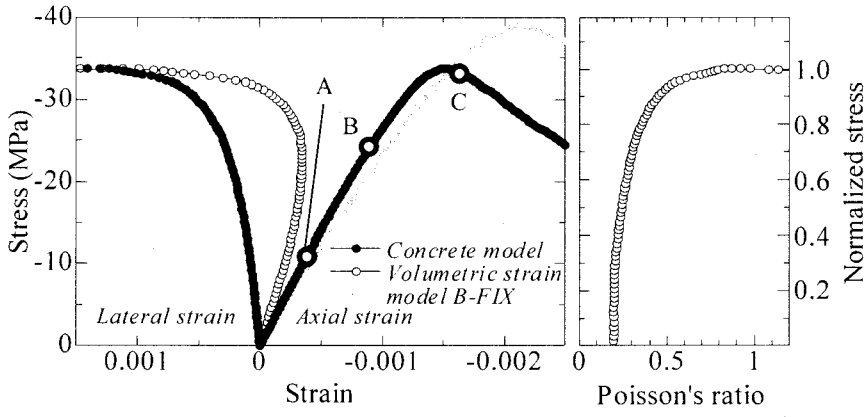

a) Stress strain curves b) Poisson's ratio

Fig. 24 Stress-strain curves

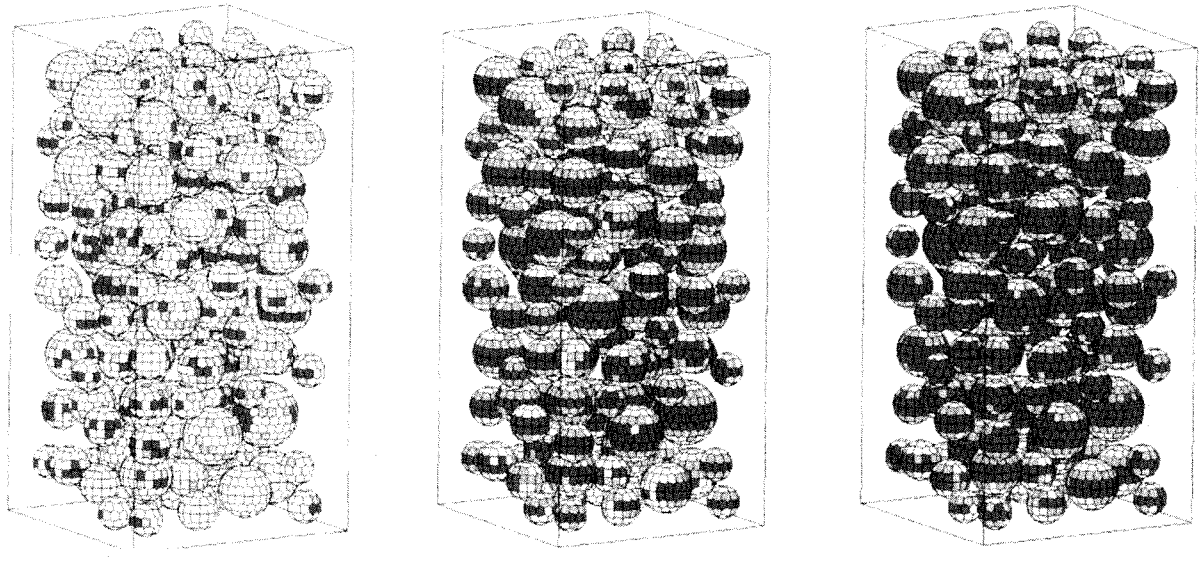

a) Point A b) Point B c) Point C

Shear stiffness decreased phase Cracked phase

Fig. 25 Changing of condition of the interface

Fig.22 shows the numerical model. Aggregate size distribution is determined based on the JSCE Standard Specification for Concrete Structures[20] and the maximum aggregate size is 20mm as shown in Fig.23. Aggregate diameters used for the analysis are varied with 2mm interval. Number of the aggregates of each size is calculated using the distribution curve in Fig.23 and points on the curve indicate the chosen diameters. Targeted aggregate volume in the model is 35%. However in this study, only the aggregates whose diameters are not less than 10mm are introduced because of the difficulty of forming sphere shape with the small size. As a result, the total aggregate volume in the model becomes 24.9%. Table 3 shows the number of the aggregate for each aggregate diameter and total number of aggregate is 167. Loading boundary in lateral direction is fixed in the simulation. Total number of element is 48,258 including 15,867 aggregate elements.

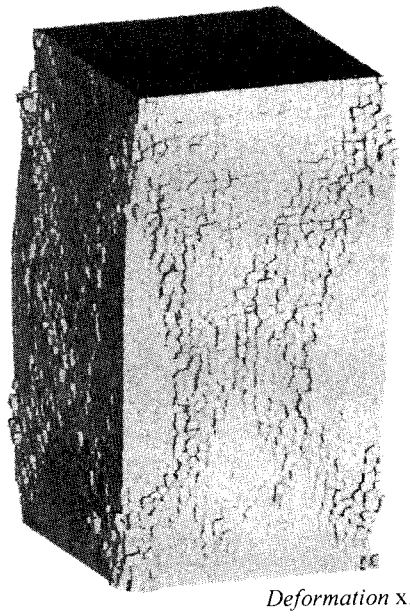

Deformation x*10*

Fig. 26 Deformation at failure

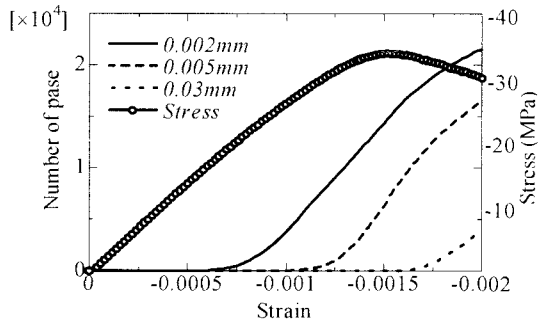

a) Interface

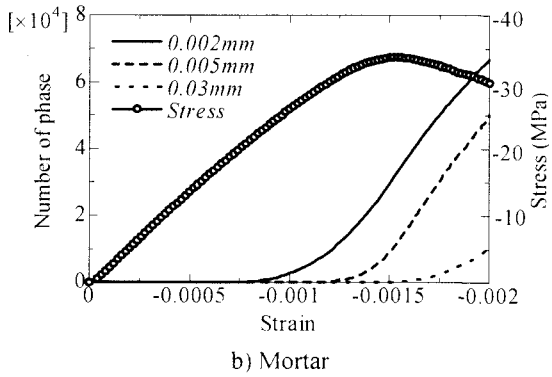

b) Mortar

Fig. 27 Number of phase reaching crack width

Fig.24 a) shows the predicted stress-strain curve and stress-volumetric strain curve of concrete model and Fig.24 b) shows the changing of Poisson's ratio of concrete model. To calculate the lateral strain and volumetric strain, relative displacement of the elements those are located on the center of the side surface of model is used. Predicted results of model B-FIX is presented as well in Fig.24 a). Strength of the concrete model is 33.67MPa. Reduction ratio of the strength due to the introduction of aggregates is 13.4%. This reduction is observed also in the experiment [3) 19) 21)]. The shapes of the curves of Poisson's ratio and volumetric strain are similar to the usual experimental results[22)]. Kosaka et al. summarized the previous researches on initiation stress of concrete that is the point that rapid increasing of Poisson's ratio is observed and critical stress of concrete that is the point that volumetric strain starts to increase from decrease[23)]. Generally, initiation stress and critical stress are 50~90% and 75~100% of strength of concrete, respectively. In the simulation, rapid increasing of Poisson's ratio is observed from around 70% of peak stress (see Fig.24 b)) and volumetric strain increase from around 25MPa that is 74% of peak stress (see Fig.24 a)). Though critical stress in simulation is slightly smaller than that in experiment, analysis can simulate the changing of Poisson's ratio and volumetric strain of concrete qualitatively.

Fig.25 shows the changing of the interface condition at A-C in Fig.24 a). Meaning of the color of the phase is same as in Fig.19 (See Section 5.1). Same as the single sphere aggregate concrete model, propagation of fracture from the side of aggregates surface is simulated. Fig.26 shows the deformation at failure (axial strain of -2,500μ). Shear crack same as usual experimental result can be simulated. Fig.27 shows the increasing of numbers of phases of the interface and mortar whose crack widths reach 0.002mm, 0.005mm and 0.03mm. The horizontal axis shows the macro-scopic strain of the model. And also macro-scopic stress is presented in the graphs. Same as the analysis of single aggregate concrete model, the interface crack increases from low stress level and the mortar crack increases rapidly from around the peak stress. However the points of crack emergence of the interface and mortar are not so different. In general, interface crack occurs in low stress level and propagates to the mortar part around the peak stress in the failure process of normal concrete. However, accurate and reliable experiment on fracture process of usual concrete has not been carried out yet. Further research is necessary from both experimental and analytical point of view.

6. Conclusions

The followings are concluded from the analyses of mortar and concrete model by three-dimensional Rigid Body Spring Model (RBSM) with meso scale elements, where only tension and shear failure of spring but compression failure is assumed.

(1) The calculated stress-strain curves of the mortar in compression show a similar shape to that in usual experimental results.

(2) Sudden increase in number of cracks in meso scale before the peak stress in the compression test of the mortar can be predicted by the analysis.

(3) Different crack patterns due to the different loading boundary conditions in the compression test can be simulated reasonably.

(4) In the tension analysis of the mortar, the localization of failure after the peak stress and the propagation of single crack can be simulated.

(5) The analysis of concrete models can present clearly fracture propagation of the interface between mortar and aggregate and stress-strain relationship which are quite similar to those in usual concrete tests.

(6) Reduction in macro compression strength of the concrete due to inclusion of aggregates can be predicted well by the analysis.

(7) Changing of Poisson's ratio and volumetric strain of concrete can be simulated qualitatively.

Acknowledgement

This research is carried out with support of the Yoshida Prize Scholarship of JSCE in 2002. The authors grateful to Prof. Yoshio KAKUTA for his valuable advise toward this study.

References

1) Yokomichi, H., Kakuta, Y. and Terasawa, S., The significant point and the fracture in deformation of concrete, *Proc. of technique on cement*, XXIV, pp.282-285, 1970. (in Japanese)

2) Trende, U. and Buyukozturk, O., Size effect of aggregate roughness in interface fracture of concrete composites, *ACI Material Journal*, July-Aug., pp.331-338, 1998.

3) Kosaka, Y., Tanigawa, H. and Kawakami, M., Effect of coarse aggregate on fracture of concrete (part 1), *Proc. of AIJ*, Vol.228, Feb., pp.1-11, 1975. (in Japanese)

4) Liu, Y. et al., Simulating mesoscopic fracture process in cement-based composites using random particle-spring systems, *JSCE Journal of Structural and Engineering*, Vol.42A, pp.247-254, 1996. (in Japanese)

5) Stroeven, P. and Stroeven, M., Space approach to concrete's space structure and its mechanical properties, *Heron*, Vol.46, No.4, pp.265-289, 2001.

6) Nagai, G., Yamada, T. and Wada, A., On a finite element procedure based on the real 3-dimensional image for concrete materials, *J. Struct. Constr. Eng.*, AIJ, No.509, July, pp.77-82, 1998. (in Japanese)

7) Asai, M. et al, Meso-scopic numerical analysis of concrete structure by a modified lattice model, *J. Struct. Mech. Earthquake Eng.*, JSCE, No.731/I-63, pp.19-30, 2003.

8) Toi, Y. and Kiyosue, T., Damage mechanics models for brittle microcracking solids based on three-dimensional mesoscopic simulations, *Engineering Fracture Mechanics*, Vol.50, No.1, pp.11-27, 1995.

9) Toi, Y. and Kiyosue, T., Three-dimensional mesomechanical analysis of brittle solids containing microinclusions, *Journal of the Japan Society of Mechanical Engineers (Series A)*, Vol.61, No.582, pp.447-453, 1995. (in Japanese)

10) Nagai, K. et al, Numerical simulation of fracture process of concrete model by Rigid Body Spring Model, *Proc. of JCI*, Vol.24, No.2, pp.163-168, 2002.

11) Nagai, K., Sato, Y. and Ueda, T., Numerical simulation of fracture process of plain concrete by Rigid Body Spring Method, *Proc. of the first fib Congress 2002 Concrete Structures in the 21st Century*, Volume 8, pp.99-106, 2002.

12) Kawai, T. and Takeuchi, N., *Discrete limit analysis program, Series of limit analysis by computer 2*, Baihukan, 1990. (in Japanese)

13) Nagai, K., Numerical simulation of fracture process of concrete model by Rigid Body Spring Method, *Master thesis of Hokkaido University*, 2002.

14) Goble, C.F. and Cohen, M.D., Influence of aggregate surface area on mechanical properties of mortar, *ACI Material Journal*, Nov.-Dec., pp.657-662, 1999.

15) Harsh, S., Shen, Z. and Darwin, D., Strain-rate sensitive behavior of cement paste and mortar in compression, *ACI Material Journal*, Sep.-Oct., pp.508-516, 1990.

16) Van Mier, J.G.M., *Fracture process of concrete*, CRC press, 1997.

17) Taylor, M.A. and Broms, B.B., Shear bond strength between coarse aggregate and cement paste or mortar, *ACI Journal*, Aug., pp939-956, 1964.

18) Hsu, T.T.C. and Slate, F.O., Tensile bond strength between aggregate and cement paste or mortar, *ACI Journal*, April, pp.465-485, 1963.

19) Christensen, P.N. and Nielsen, T.P.H., Modal deformation of the effect of bond between coarse aggregate and mortar on the compressive strength of concrete, *ACI Journal*, Jan., pp.69-72, 1969.

20) *Standard specification for concrete structures - 2002, Materials and construction*, JSCE, March, 2002. (in Japanese)

21) Stock, A.F., Hannant, D.J. and Williams, R.I.T., The effect of aggregate concentration upon the strength and modulus of elasticity of concrete, *Magazine of concrete research*, Vol.31, No.109, Dec., pp.225-234, 1979.

22) *Concrete handbook – Japan Concrete Institute edition*, Gihodo, 1976. (in Japanese)
23) Kosaka, Y., Tanigawa, H. and Kawakami, M., Effect of coarse aggregate on fracture of concrete (part 3), *Proc. of AIJ*, Vol.233, July, pp.21-32, 1975. (in Japanese)

(Received September 12,2003)